НАУЧНО-ТЕХНИЧЕСКИЙ ВЕСТНИК ИНФОРМАЦИОННЫХ ТЕХНОЛОГИЙ, МЕХАНИКИ И ОПТИКИ
май–июнь 2023 Том 23 № 3 http://ntv.ifmo.ru/
SCIENTIFIC AND TECHNICAL JOURNAL OF INFORMATION TECHNOLOGIES, MECHANICS AND OPTICS
May–June 2023 Vol. 23 No 3 http://ntv.ifmo.ru/en/
ISSN 2226-1494 (print) ISSN 2500-0373 (online)

doi: 10.17586/2226-1494-2023-23-3-575-584

Blindness detection in diabetic retinopathy using Bayesian variant-based connected component algorithm in Keras and TensorFlow

Shanmugavel Anantha Babu[1], Subramanian Murali[2], Ellappan Vijayan[3], Mahendran Anand[4], Lakshmanan Ramanathan[5]✉

[1] Koneru Lakshmaiah Education Foundation, Hyderabad, 500075, Telangana, India
[2,3,4,5] Vellore Institute of Technology, Vellore, 632014, India

[1] ananthmtech@gmail.com, https://orcid.org/0000-0002-7446-0283
[2] murali.s@vit.ac.in, https://orcid.org/0000-0002-1631-8078
[3] evijayan@vit.ac.in, https://orcid.org/0000-0002-0207-0411
[4] manand@vit.ac.in, https://orcid.org/0000-0002-7629-9606
[5] lramanathan@vit.ac.in✉, https://orcid.org/0000-0002-1532-5495

Abstract

The neuro-degenerative eye disease glaucoma is caused by an increase in eye pressure inside the retina. As the second-leading cause of blindness in the world, if an early diagnosis is not obtained, this can cause total blindness. Regarding this fundamental problem, there is a huge need to create a system that can function well without a lot of equipment, highly qualified medical personnel, and takes less time. The proposed modeling consists of three stages: pre-training, fine-tuning and inference. The probabilistic based pixel identification (Bayesian variant) predicts the severity of Diabetic Retinopathy (DR) which is diagnosed by the presence of visual cues, such as abnormal blood vessels, hard exudates, and cotton wool spots. The article combines machine learning, deep learning, and methods for image processing to predict the diagnosis images. The input picture is validated using Bayesian variant connected component architecture, and the brightest spot algorithm is applied to detect the Region of Interest (ROI). Moreover, the training sample calculated optic disc and optic cup are segmented with fundus photography ranges 0 to 4 using VGGNet16 architecture and SMOTE algorithm to detect DR stages of images and the proposed model using ensemble based ResNet with Efficient Net produces the excellent accuracy score of 93 % and predicted image Kappa coefficient ($p < 0.01$) 0.755 of the fundus retina image dataset.

Keywords

Bayesian variant, Keras and TensorFlow, ensemble learning, EfficientNet, ResNet

For citation: Anantha Babu S., Murali S., Vijayan E., Anand M., Ramanathan L. Blindness detection in diabetic retinopathy using Bayesian variant-based connected component algorithm in Keras and TensorFlow. *Scientific and Technical Journal of Information Technologies, Mechanics and Optics*, 2023, vol. 23, no. 3, pp. 575–584. doi: 10.17586/2226-1494-2023-23-3-575-584

УДК 004.89

Обнаружение слепоты при диабетической ретинопатии с использованием алгоритма связанных компонентов на основе байесовского варианта в Keras и TensorFlow

Шанмугавел Ананта Бабу[1], Субраманиан Мурали[2], Эллаппан Виджаян[3], Махендран Ананд[4], Лакшманан Раманатан[5]✉

[1] Университет Конеру Лакшмайан (KL), Хайдарабад, 500075, шт. Телангана, Индия
[2,3,4,5] Технологический институт Веллуру, Веллуру, 632014, Индия

[1] ananthmtech@gmail.com, https://orcid.org/0000-0002-7446-0283
[2] murali.s@vit.ac.in, https://orcid.org/0000-0002-1631-8078
[3] evijayan@vit.ac.in, https://orcid.org/0000-0002-0207-0411
[4] manand@vit.ac.in, https://orcid.org/0000-0002-7629-9606
[5] lramanathan@vit.ac.in✉, https://orcid.org/0000-0002-1532-5495

Аннотация

Нейродегенеративное заболевание глаз — глаукома, вызывается повышением внутриглазного давления сетчатки. Это вторая по значимости причина слепоты в мире. Отсутствие раннего диагноза приводит к полной слепоте. Актуальной проблемой является создание системы диагностики, которая может функционировать без большого количества оборудования, высококвалифицированного медицинского персонала и занимает мало времени. Предложенное в работе моделирование состоит из трех этапов: предварительная подготовка, тонкая настройка и логический вывод. Вероятностная пиксельная идентификация (байесовский вариант) позволяет прогнозировать тяжесть заболевания по наличию визуальных признаков, таких как аномалия кровеносных сосудов, наличие твердых экссудатов и ватообразных очагов. Рассмотрено сочетание машинного обучения, глубокого обучения и методов обработки изображений для оценки и идентификации диагностических изображений. Входное изображение проверено с использованием байесовской архитектуры связанных компонентов. Для обнаружения области интереса (ROI) применен алгоритм наиболее яркого пятна. Для обнаружения стадий диабетической ретинопатии по фотографиям глазного дна выполнены расчеты диска и чаши зрительного нерва. Изображения сегментированы от 0 до 4 с использованием архитектуры VGGNet16 и алгоритма SMOTE. Представленная модель с применением алгоритма ResNet на основе ансамбля с Efficient Net дала оценку точности 93 % и предсказанный коэффициент Каппа изображения ($p < 0{,}01$) 0,755 набора данных изображения сетчатки глазного дна.

Ключевые слова

байесовский вариант, Keras и TensorFlow, ансамблевое обучение, EfficientNet, ResNet

Ссылка для цитирования: Ананта Бабу Ш., Мурали С., Виджаян Э., Ананд М., Раманатан Л. Обнаружение слепоты при диабетической ретинопатии с использованием алгоритма связанных компонентов на основе байесовского варианта в Keras и TensorFlow // Научно-технический вестник информационных технологий, механики и оптики. 2023. Т. 23, № 3. С. 575–584 (на англ. яз.). doi: 10.17586/2226-1494-2023-23-3-575-584

Introduction

Recently, diabetes affects roughly 250 million individuals worldwide. People with diabetes have elevated blood glucose levels and their retinas suffer as a result. Loss of eyesight or blindness results from this. The leading causes of blindness and visual impairment in humans are Diabetic Retinopathy (DR), glaucoma, age-related macular degeneration, and cataract. The most well-known form of DR is diabetic blindness [1]. As a result, the blood vessels in the retina are damaged, which can lead to blindness. One in four people with the same type of DR, which affects up to 4.1 million individuals, have visual loss. A process known as DR damages the blood vessels in the retina, a luminous tissue located in the back of the eye [2]. Diabetes is a major cause of vision loss in diabetics and is one of the main risk factors for vision loss and blindness in persons below the age of 70. Most diabetic may get retinopathy which can be very severe since that raises the possibility of blindness if untreated. Regular eye exams are crucial to getting the problem treated while it is still treatable since it is easiest to do this in the initial stages. We have scanned images to utilize trained surgeons to diagnose the illness instead of automation system.

— It benefits the patient, particularly those who cannot afford medical care.
— It lessens human effort, particularly when there are fewer specialists.
— It is useful for persons living in remote locations where medical screening is challenging to perform.
— It reduces the amount of time needed to diagnose an illness.

Diabetic screening aids in the early detection of the disease asymptomatic phases and can be modified to result in effective therapy. This makes it possible for medical providers to use screening in rural and isolated locations where specialist healthcare is lacking. In medical image analysis, the location of structures must be determined. Visual acuity is in danger when the background alterations take place in the central retina, a disease known as diabetic maculopathy. Unfortunately, many people go misdiagnosed even as their diabetes severely destroys their retinas since sight loss is frequently a late indication of advanced diabetic maculopathy [3].

A condition known as glaucoma (Gl) affects the optic nerve which connects the eye to the brain. The optic nerve is compromised when Intraocular Pressure (IOP), often known as eye pressure, is high [4]. A rise in blood sugar doubles the likelihood of Gl which if left untreated can result in blindness and visual loss. Based on the size of the swollen optic nerve head or optic disc and Cup-to-Disc Ratio, or cupping, Gl may be divided into three categories: there exist mild, moderate, and severe Gl phases [5]. Diabetic Macular Edema is a fluid buildup in the macular region of the retina brought on by blood vessel destruction. Straight-ahead vision is made crisp by the macula. The macula swells and thickens as a result of fluid accumulation causing visual distortion. Based on the following criteria, mild, moderate, and severe Diabetic Macular Edema phases can be distinguished [6].

The major goals of the proposed study are to improve sensitivity, specificity, and accuracy of DR diagnosis by detecting blood vessels, microaneurysms, hemorrhages, and exudates. To create an automatic grading system for various DR phases that is highly accurate and requires little computational effort.

Literature Review

Systems for analyzing retinal images have the ability to process data through image processing and machine learning techniques. There are various uses of image processing algorithms in the literature for diagnosing retinal disorders [7]. The early digital retina fundus images were classified using manually derived features and empirically determined parameters. According to the authors, computer

vision techniques may now be used to automatically find microaneurysms system. Eight characteristics among pixel area and total pixel intensity, recorded for each candidate, were used in their studies using simple morphological and thresholding procedures [8]. The suggested approach produced outcomes equivalent to those attained by medical professionals demonstrating the diagnostic utility of automated lesion identification. Images may be visualized using a variety of image-processing tools and techniques [9, 10]. The photos are subjected to several pre-processing procedures to improve their visualization. A network may pick up more superior qualities when the images are brighter and clearer. We will make a quick mention of the image processing methods employed by the writers and researchers in this part. Compared to the other channels, the Green channel in the RGB color space offers more contrast and information [11].

The chronic damage to the optic nerve caused by the degenerative eye disease glaucoma eventually results in permanent blindness and a loss of visual field. It is the second most common explanation for glaucoma. According to the widely used model, 11.1 million individuals would have glaucoma globally in 2020 [12]. IOP, or elevated Intraocular Pressure, is a primary factor in damage to thefragile nerve fibres of the optic nerve. Glaucoma can occasionally occur in individuals with IOP levels within the normal range. IOP in glaucoma sufferers is greater than 20 mmHg (normal IOP is 10 mmHg), which might harm the optic nerve in the back of the eye and result in blindness [13].

In order to acquire unsupervised features and categories patterns, Deep Learning (DL), a subset of machine learning techniques, uses hierarchical layers of non-linear processing stages [14]. One technique for computer-assisted medical diagnosis is DL. Classification, segmentation, detection, retrieval, and registration of the pictures are only a few of the DL applications used in medical image analysis. Convolutional Neural Networks (CNNs) are employed more frequently than the other techniques in medical image analysis [15], and they are also quite successful. Convolution layers (CONV), pooling layers, and fully linked layers make up the three basic levels of the CNN architecture (Fully Connected). Depending on the author's vision, the CNNs size, number of filters, and layer count can change. In the CNN design, each layer has a distinct function. Different filters convolve a picture to extract its characteristics in the CONV layers. In order to shrink the size of feature maps, the pooling layer is often applied after the CONV layer. There are several pooling algorithms; however average pooling and maximum pooling are most often used [16].

Residual representations

VLAD [17] is a format for image recognition that encodes using residual vectors in relation to a dictionary, and Fisher Vector can be in the form of a probabilistic VLAD formulation.

Strong shallow models for vision classification and retrieval are among them. Vector quantization has demonstrated that residual vector encoding is more efficient than original vector processing.

An essential method for examining the retina arteries and veins is retinal vascular segmentation [17]. Blood vessel segmentation is essential in this sort of analytic method which is used by various medical professions to discover a variety of medical concerns. Due to the significance of fundus vessels, several fundus vascular segmentation techniques have been developed over time [18]. The results of a manual segmentation might be regarded as the accurate results. Although manual segmentation is easy, it is a laborious operation. Additionally, fatigue makes it more prone to mistakes [19]. Additionally, because each person may interpret the image differently, there can be some variations in the segmentation findings from various individuals. Therefore, a simpler and more efficient segmentation method should be developed.

A type of machine learning technique known as "unsupervised learning" is used to draw conclusions from data sets that contain input data without labeled replies. In unsupervised learning the approaches were discussed. According to a method proposed by Zhao et al. [20] for segmenting retinal blood vessels, based on the level set and region growing method, the extracted green channel image is first enhanced using CLAHE and a 2D Gabor wavelet transform before being smoothed out with an anisotropic diffusion filter that maintains the vessel boundary [21].

While UNet architectures may keep the image structural integrity, they are more suited for semantic segmentation than conventional CNNs. They include a contracting path to collect the pertinent context and an expanding path that is symmetrical allowing for exact segmentation. Additionally, UNet architecture processes the image in a single pass rather than processing various patches in a sliding window approach as a CNN would that is why such architectures are referred to as "Fully Convolutional Networks" (FCN) [22] and also have number of parameters and are faster than conventional CNNs.

System Model

The essential components of CNNs will be discussed in detail in this article. Fully linked layers, also known as traditional neural networks, are presumed to be recognizable to the reader based on this. The basic units of neural networks in the past have been matrix multiplications and nonlinearities like sigmoid. These levels of a matrix multiplication are now known as fully-connected layers since every unit in the layer below it is connected to every unit in the layer. In our model, a free library named TensorFlow is accessible on GitHub. When it comes to work with Deep Neural Networks, it is one of the more well-known libraries. On top of Theano or TensorFlow, Keras is a high-level library. It offers a scikit-learn-style Python API for creating neural networks. The primary motive behind the creation of Keras is to make experimenting easier through rapid prototyping.

Bayesian variant

By using deep learning method, a probabilistic pixel-by-pixel segmentation model known as the "Bayesian" network was developed as an alternative to the original network. With the help of this technology, it is feasible to do probabilistic pixel-wise categorization using drop-

out and Monte Carlo sampling. Determine the posterior distribution (P) over the convolutional weights w using the actual training data x and labels z as inputs.

$$P(w|x, z).$$

The Kullback-Leibler divergence between the targeted approximation distribution and the complete Bayesian probability is eliminated.

$$I(x, y) = klP(x, y)||P(x)P(y).$$

I denotes the input image and we applied kl as divergence Bayesian probability. The posterior distribution over the weights would be sampled at test time to create the distribution of softmax class probabilities. Convolutional kernel sizes were set at 3 × 3 for the Original network and 7 × 7 for both of the Basic networks to provide a broad context for smooth labelling. We trained our networks using a stochastic Bayesian network model that integrates raw data from color, edge map, and texture in order to improve the accuracy of content-based photo retrieval systems.

Bayesian classifier

We consider k classes, ω_1, ω_2, …, ω_k, with the prior probability P_i, $i = \overline{1, k}$, $X = \{X_1, X_2, \ldots, X_n\}$ is the n-dimensional continuous data with $x = \{X_1, X_2, \ldots, X_n\}$ being a specific sample. According to [23], a new observation x belongs to the class ω_1 if and only if

$$P(\omega_i|x) > P(\omega_j|x) \; for \; 1 \le j \le k, j \ne k.$$

In the continuous case $P(\omega_i|x)$, is calculated by

$$P(\omega_i|x) = \frac{P(\omega_i)f(x|\omega_i)}{\sum_{i=1}^{n} P(\omega_i)f(x|\omega_i)} = \frac{P_i f_i(x)}{f(x)}.$$

Connected components

Through pixel-by-pixel analysis of an image, linked component labelling finds related pixel areas, or regions of nearby pixels, that have the same set of intensity values V as connected componets. (from top to bottom and left to right). (V is always 1, despite the fact that V may take on multiple values in a grayscale image.)

Let ∂s be a neighbourhood system:

— 4-point neighbourhood system,

— 8-point neighbourhood system.

Let c(s) denote the collection of nearby points s that are linked together, i.e., set of pixels. The set c(s) for all s(set) and r must possess the characteristics that — c(s) ⊂ ∂s – – $r \in$ c(s) ⇔ $s \in$ c(r) radius. In general, calculating c(s) may be very difficult. Use the following pseudocode to find a linked set by growing an area from a seed point.

Pseudo Code: *Connected Set Growing Region*

```
ClassLabel = 1
Initialize Yr = 0 for all r ∈ S
ConnectedSet(s0, Y, ClassLabel) {
 B ← {s0}
 While B is not empty {
 s ← any element of B
 B ← B − {s} Ys ← ClassLabel
 B ← B S {r : r ∈ c(s) and Yr = 0
 }
 }
 return(Y)
}
```

The proposed model, after enlarging the region to the nearest pixel, applies the extract the corresponding component sets to cycle through each pixel in the image. For each pixel that isn't labeled, an associated set should be extracted.

Pseudo Code: *Extract the connected components Region*

```
ClassLabel = 1
Initialize Yr = 0 for r ∈ S
For each s ∈ S {
 if(Ys = 0) {
 ConnectedSet(s, Y, ClassLabel)
 ClassLabel ← ClassLabel + 1
 } }
```

Proposed Procedures

Fig. 1 depicts the finalized proposed Bayesian version based on linked components to identify the diseases in the eye dataset. In large collections of misclassification data, the ensemble model may be optimized and used with ResNet. The next part provides information on the proposed training and testing dataset for employing the linked components based on the Bayesian variation.

Proposed algorithm

Step 1: Read *APTIOS* retina data set collected from *Kaggle*.

Step 2: To determine whether an input (x) coincides with a label, evaluate your network input data in the first phase (y). Make that the ground-truth label (y) is suitably encoded to label indexes, assuming dense prediction.

Step 3: A pre-trained model should be chosen based on how well it is handled hyper parameters.

Step 4: After convolution layers, add Dropout layers, modify a few layers, or train the classifier using a small dataset.

Step 5: During training, employ class weights if the data issue is extremely uneven. Alternatively, give the unusual class more weight while reducing the weight of the main class.

Step 6: Utilize Max-pooling to cut down on computations before ReLU. ReLU thresholds zero-valued values. Max-pooling only pools the maximum activations when $f(x) = \max(0, x)$: Use Conv > MaxPool > ReLU when $f(x) = \max(x_1, x_2, ..., x_i)$ Conv > ReLU > MaxPool is preferred.

Step 7: Use 80–20 for training and testing the ML Bayesian Variant + Connected Component model to forecast the model.

Step 9: To evaluate the correctness of the provided dataset, use the confusion matrix.

Step 10: Finally, provide a categorization report with accuracy, recall, and precision.

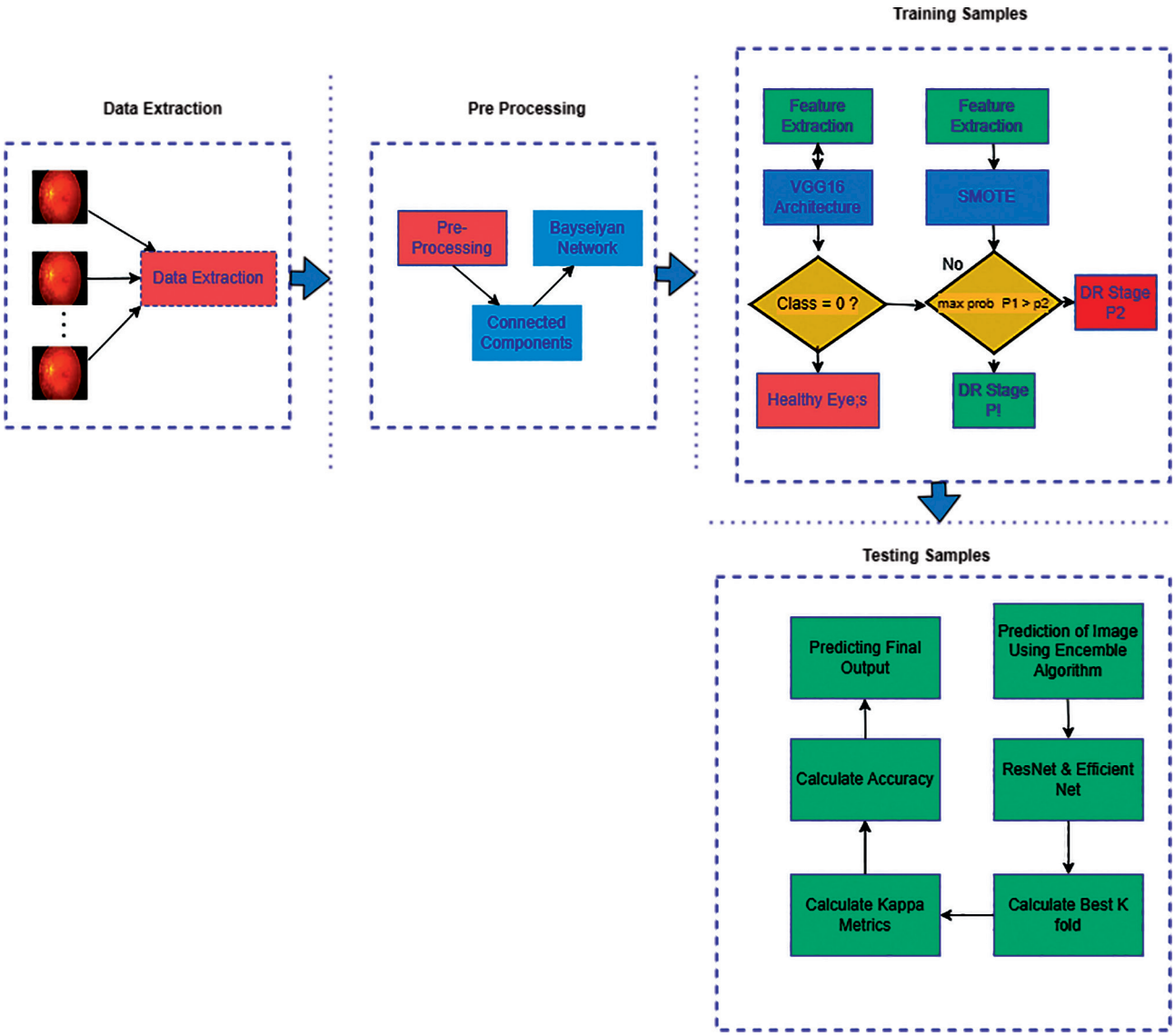

Fig. 1. Bayesian Variant-Based Connected Component Model

Results and Discussion

Pre-processing

Pre-processing the data is an important step that is frequently missed. The caliber of the input is the crucial step of preprocessing the data which is routinely skipped. The effectiveness of the produced machine learning models is significantly influenced by the quality of the input data. Before beginning the modeling process, it is crucial to analyze the data and to take into consideration any potential problems. The material consists of 3662 retinal photographs of clinical patients with labels and 1928 retinal photographs with test labels. A clinical expert assigns labels to the photographs. The severity of DR is denoted by numerical labels on a range from 0 to 4, with 0 denoting no illness and 4 denoting the proliferative stage of DR. It is based on how successfully a pre-trained model handled by hyper-parameters and should select it. Fig. 2 shows the distribution of the classes for the data gathered from the "train.csv" and "sample submission.csv" files. Since different camera models were used to gather the information from various clinics, there are variations in the image resolution, aspect ratio, and other factors.

Images of 49 % of the patients suggest that they are in good health, according to the imbalance data. The remaining 51 % are stages of DR. With just 5 % of instances falling into Class 3 (the severe stage), it is the least frequent. Because different camera types were utilized to capture the data, the picture resolution, aspect ratio, and other elements of the data from the various clinics vary.

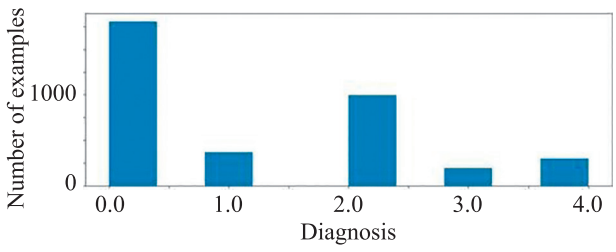

Fig. 2. Class distribution of Blindness Detection Model (524 × 197 px)

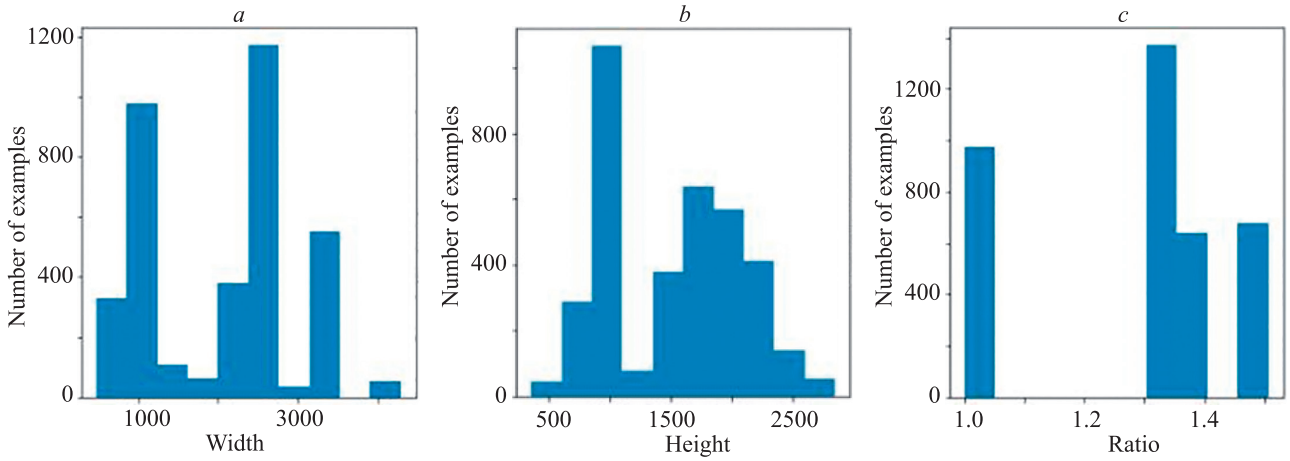

Fig. 3. Image: width (276 × 288 px) (*a*); height (276 × 288 px) (*b*); ratio (276 × 288 px) (*c*)

The following example shows how to accomplish this by plotting the histograms of the images width, height, and aspect ratio. Fig. 3 shows, observation of trained dataset images with calculations of width, height and image ratio. X-axis of each image are width, height and ratio.

In Fig. 3, height and width are observed from the total number of observation images. The ratio is calculated with total number of image width divided by total number of image height. The severity of DR is assessed visually using indicators including abnormal blood vessels, hard exudates, and so-called cotton wool patches. Comparing the examples, we can see that some of the retinal pictures of the sick people include cotton wool patches and exudates.

Bayesian network model training

Although just 2 % of the photos depict the most advanced stage of the DR, the gap between the source and goal data is more pronounced: 73 % of the photos depict healthy individuals while the goal data only contains 2 % of such images. To balance things out during training, we'll use a sample from the target data set as a validation sample. To support different enhancements on the training and inference stages, the model produces two "Dataset" objects, "EyeTrainData" and "EyeTestData". A random crop is present but not included in the test data in the first case. Fig. 4 shows augmented training images.

The leading edge of CNN performance is in computer vision tasks. Recent medical research also shows that CNNs with DR categorization have a lot of potential. The CNN EfficientNet & ResNet model architecture is utilized in this study. It contains 8 different architectures, ranging from B0 to B7, with different default picture sizes and levels of model complexity. The non-linear, unsupervised approach used in t-Distributed Stochastic Neighbor Embedding (t-SNE) is primarily used for high-dimensional data visualization and data exploration. If the values of the data points x_1 and x_2 are same beneath this Gaussian circle, which denotes that their proportions and similarities are likewise equivalent, then there are local similarities in the structure of this high-dimensional space. The Gaussian distribution or circle may be altered using the idea of complexity which effectively influences the number of closest neighbors and the variance of the distribution (circle size). We can greatly improve the sharpness of the characteristics and visual details in the eye by using Gaussian blur.

The Gaussian blur feature is created by blurring (or smoothing) a photo using a Gaussian function to reduce noise. After resizing the image, we enhanced it using Gaussian blur. We removed the extraneous features and kept just the relevant parts of the image. Bilinear interpolation was used to scale the photos. Fig. 5 presents the result after applying Gaussian blur image.

$$I_{norm} = \frac{I - \min(I)}{\max(I) - \min(I)}.$$

In the formula, I represents normalization of the given image used to remove the dark area of images. The retina image was converted to grayscale, and a tolerance value larger than 7 was decided upon in order to create a mask. The picture primary goal was to get any dark areas totally removed. For the X and Y axes, we decide to utilize a standard deviation of 10. Each point in the input vector was concatenated and added using a Gaussian kernel to produce the output image:

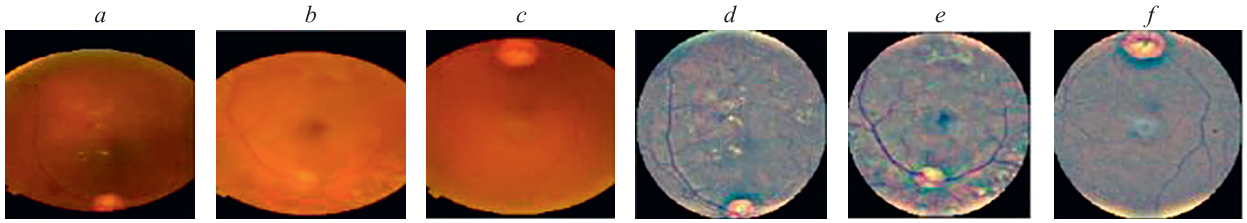

Fig. 4. Augmented Training Images: 112 × 112 px (*a*); 110 × 110 px (*b*); 112 × 113 px (*c*); 113 × 112 px (*d*,*f*); 113 × 116 px (*e*)

$$G(x) = \frac{1}{\sqrt{2\pi\sigma^2}} e^{\frac{-x^2}{2\sigma^2}}.$$

Using this equation, the original and blurred pictures were merged. Parameter σ is determined by single scaling parameter when using it to describe the scale towards directions, the propagation of blurriness is model as circular shape; x is referred as training set of the images. Now represent $G(x)$ as Gaussian image:

$$G(x) = (1 - \alpha)f_0(x) + \alpha f_1(x),$$

where f_0 is original image and f_1 represents noisy image. To get the desired image, we assign the value of $\alpha = 4$, $\beta = 4$, and free term $\gamma = 128$ for the programme which produced the finished image:

$$dst = \alpha img1 + \beta img2 + \gamma.$$

The final pre-processed image utilized in the training model is shown in Fig. 6. Each fundus picture underwent pre-processing to make the features and nerves more prominent and to eliminate the background dark region to cut down on unnecessary data.

Class "0" is distinguishable from other classes by the model (1–4). Separating grades 1–4 seems to be a challenge. After being reduced to 1D and flattened to 2D grayscale, t-SNE (t-distributed Stochastic Neighbour Embedding) is applied. When working with CNN extracted features, t-SNE also is effective. With t-SNE, to create maps that illustrate which input data the network considers to be "similar". Fig. 7, *a* shows the distribution of t-SNE for perplexity = 5 and Fig. 7, *b* presents t-SNE for perplexity = 10.

Evaluation parameters

Kappa Score is computed based on the precision parameter pre-trained weights for efficient net. After 0 to 4 training every bucket epochs, depending on a fold, the best validation performance is reached; this shows

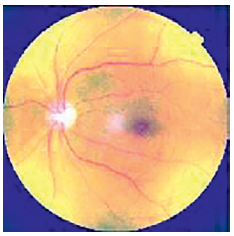

Fig. 5. After Applying Gaussian Blur (174 × 174 px)

Fig. 6. After Applying Crop and Gaussian Blur (180 × 178 px)

improved performance in categorising mild stages of DR. A classification outcome based on pixels is produced by retinal vascular identification utilising linked components and the Bayesian version. Either the background or the vessel is assigned to each pixel. After 3 epochs, the cross-entropy loss on the validation set is at its lowest. Kappa keeps rising over this time period, reaching the 8th epoch. We utilise kappa to evaluate the performance of our solution, thus we keep weights for 0 to 4 epochs. The confusion matrix of the trained model is also generated. The percentages are represented by the numbers in the cells. According to the findings, the model is unable to differentiate between the mild and moderate phases of DR: images with mild DR are classified as moderate in 86 % of instances. Those who are in good health achieve the best results. Overall, the model frequently conflates closely related severity stages while misclassifying the prolific and

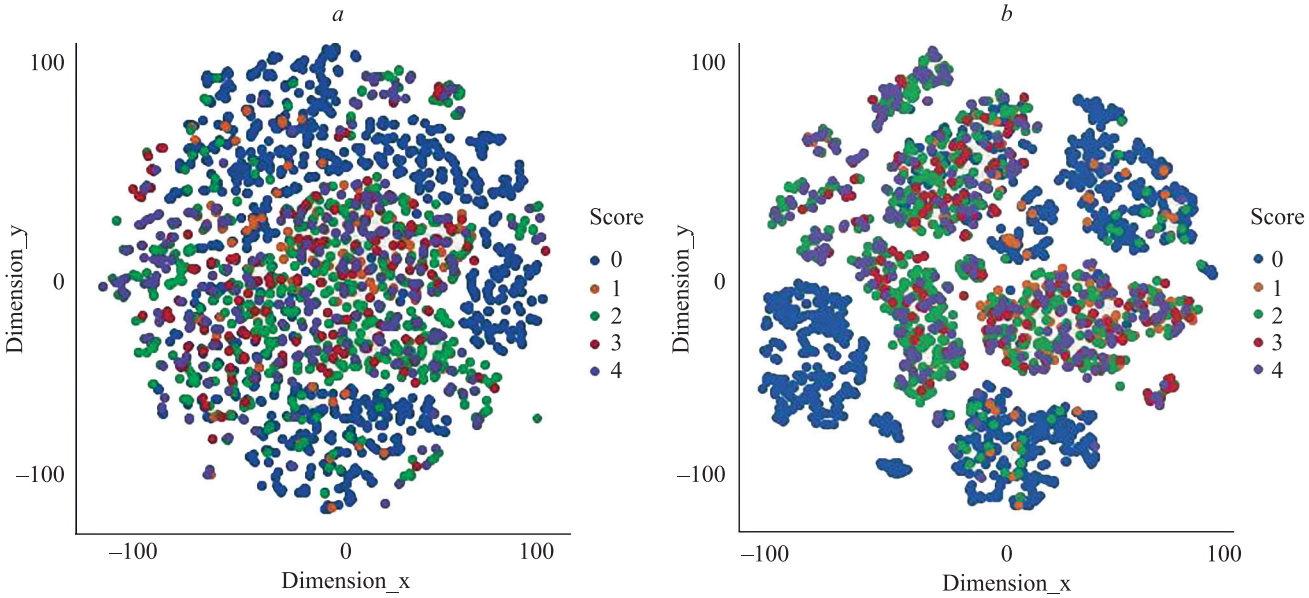

Fig. 7. TSNE Cluster Separation: perplexity = 5 (495 × 432 px) (*a*) and perplexity = 10 (463 × 436 px) (*b*)

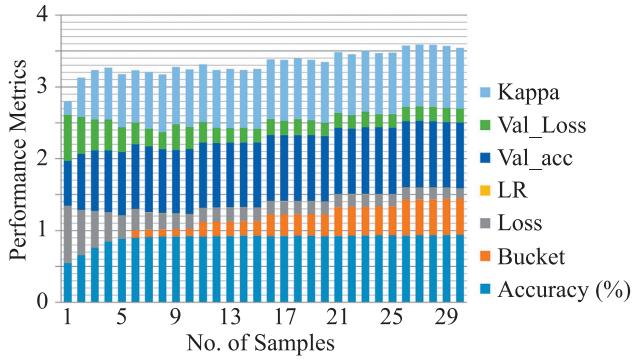

Fig. 8. Bayesian variant based EfficientNet & ResNet with Pre-trained Weights for Accuracy, Loss and Kappa Score

moderate levels. Fig. 8 shows the loss, accuracy, and Kappa score of pre-trained images; Fig. 9 presents the confusion matrix of given samples.

Comparative analysis

CNNs are commonly constructed using fewer resources then scaled up to perform better with more resources. There are several approaches to scale a model, such as arbitrarily increasing CNN depth or breadth, or employing high-resolution input images during training to capture data correlations in detail. In order to ensure the compatibility of the learned Bayesian variant with Resnet and Efficient Net models, the training test Kappa score performed with a 0.755 with an excellent accuracy rate. A minimum mean squared value and excellent kappa train by the recommended method, it has been noticed.

The quadratic weighted kappa calculated as follows. To begin, a $N \times N$ histogram matrix $\mathbf{O}$ is built, where $\mathbf{O}_{i,j}$ represents the number of installation ids (actual) that really got a value of j. Based on the difference between the actual

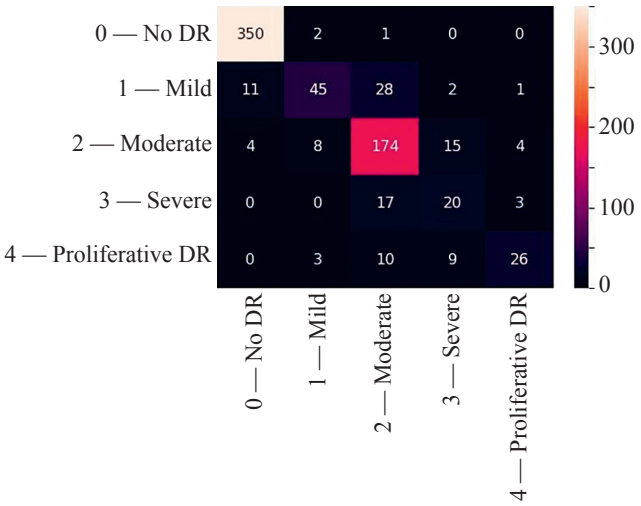

Fig. 9. Confusion Matrix (619 × 468 px)

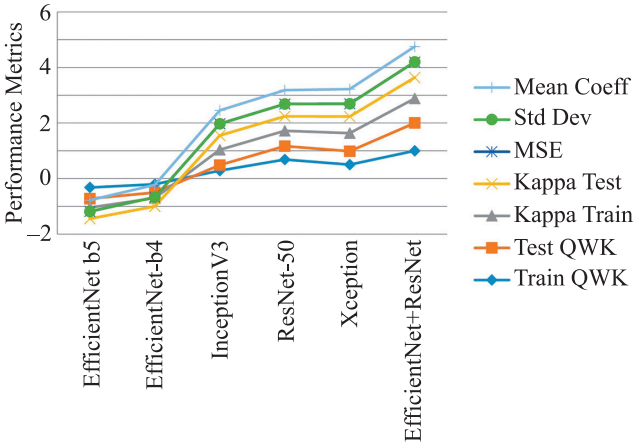

Fig. 10. Compare performance metrics in graphical analysis with other existing methods

and anticipated values, an N by N weights matrix, $\boldsymbol{\omega}$, is generated.

$$\boldsymbol{\omega}_i = \frac{(\mathbf{Q}_i - \mathbf{Q}_j)^2}{(N-1)^2}.$$

Assuming that there is no connection between values, a histogram matrix of anticipated results, N by N, is constructed as $\mathbf{E}$. This is determined by taking the outer product normalized such that $\mathbf{E}$ and $\mathbf{O}$ have the same sum between the expected and actual histogram vectors of outcomes. Where $\mathbf{O}_i$ represents actual image and $\mathbf{O}_j$ indicates anticipated values.

$$Kappa = 1 - \frac{\sum_{i,j} \boldsymbol{\omega}_{i,j} \mathbf{O}_{i,j}}{\sum_{i,j} \boldsymbol{\omega}_{i,j} \mathbf{E}_{i,j}}.$$

The quadratic weighted kappa score is a proportion that ranges from –1 to 1. The model is "worse than random" if the Quadratic Weighted Kappa (QWK) score is negative. The result of a random model should be close to 0. Our proposed model predicts the kappa score close to 0.88 to 1.00 expected random possibilities; the suggested method passed testing in Fig. 10.

Conclusion

After reviewing the results using a confusion matrix, an accuracy calculation was performed. Blood vessels scored higher after being converted to frequency. Inferred from the data, blood vessels and frequency transformations are the two characteristics that are most reliable for detecting relationships between illnesses. The model applies transfer learning to modify the newest CNN model by integrating EfficientNet with ResNet. K-fold study to obtain the best EPOCS fit revealed that the recommended model considerably enhances the classification model test time and prediction performance.

References

1. Stitt A.W., Curtis T.M., Chen M., Medina R.J., McKay G.J., Jenkins A., Gardiner T.A., Lyons T.J., Hammes H.-P., Simó R., Lois N. The progress in understanding and treatment of diabetic retinopathy. *Progress in Retinal and Eye Research*, 2016, vol. 51, pp. 156–186. https://doi.org/10.1016/j.preteyeres.2015.08.001
2. Mahmoud M.H., Alamery S., Fouad H., Altinawi A., Youssef A.E. An automatic detection system of diabetic retinopathy using a hybrid inductive machine learning algorithm. *Personal and Ubiquitous Computing*, 2021, pp. 1–15. https://doi.org/10.1007/s00779-020-01519-8
3. Dai L., Wu L., Li H., Cai C., Wu Q., Kong H., Liu R., Wang X., Hou X., Liu Y., Long X., Wen Y., Lu L., Shen Y., Chen Y., Shen D., Yang X., Zou H., Sheng B., Jia W. A deep learning system for detecting diabetic retinopathy across the disease spectrum. *Nature Communications*, 2021, vol. 12, no. 1, pp. 3242. https://doi.org/10.1038/s41467-021-23458-5
4. Leung D.Y.L., Tham C.C. Normal-tension glaucoma: Current concepts and approaches — A review. *Clinical & Experimental Ophthalmology*, 2022, vol. 50, no. 2, pp. 247–259. https://doi.org/10.1111/ceo.14043
5. French J.A., Lawson J.A., Yapici Z., Ikeda H., Polster T., Nabbout R., Curatolo P., de Vries P.J., Dlugos D.J., Berkowitz N., Voi M., Peyrard S., Pelov D., Franz D.N. Adjunctive everolimus therapy for treatment-resistant focal-onset seizures associated with tuberous sclerosis (EXIST-3): a phase 3, randomised, double-blind, placebo-controlled study. *The Lancet*, 2016, vol. 388, no. 10056, pp. 2153–2163. https://doi.org/10.1016/s0140-6736(16)31419-2
6. Nazir T., Nawaz M., Rashid J., Mahum R., Masood M., Mehmood A., Ali F., Kim J., Kwon H.-Y., Hussain A. Detection of diabetic eye disease from retinal images using a deep learning based CenterNet model. *Sensors*, 2021, vol. 21, no. 16, pp. 5283. https://doi.org/10.3390/s21165283
7. Barros D., Moura J.C., Freire C.R., Taleb A.C., Valentim R.A., Morais P.S. Machine learning applied to retinal image processing for glaucoma detection: review and perspective. *BioMedical Engineering OnLine*, 2020, vol. 19, no. 1, pp. 20. https://doi.org/10.1186/s12938-020-00767-2
8. Ray J.S.R., Babu S.A., James J.W., Vedaiyan R. ARIMA based Time Series Analysis: Forecast COVID-19 Most Vaccinated Process and Active Cases classify using Probability Distribution Curve Rates (ARIMAPDC). *Proc. of the 2nd International Conference on Smart Electronics and Communication (ICOSEC)*, 2021, pp. 546–551. https://doi.org/10.1109/ICOSEC51865.2021.9591774
9. Raj R.J.S., Babu Anantha S., Jegatheesan A., Arul Xavier V.M. A GAN-based triplet FaceNet detection algorithm using deep face recognition for autism child. *Lecture Notes in Electrical Engineering*, 2022, vol. 905, pp. 177–187. https://doi.org/10.1007/978-981-19-2177-3_18
10. Babu S.A., Joshua Samuel Raj R., Varalatchoumy M., Gopila M., Febiyola Justin B.V. Novel approach for predicting COVID-19 symptoms using ARM based APRIORI algorithm. *Proc. of the 6th International Conference on Computing Methodologies and Communication (ICCMC)*, 2022, pp. 1577–1580. https://doi.org/10.1109/ICCMC53470.2022.9753987
11. Khojasteh P., Aliahmad B., Kumar D.K. A novel color space of fundus images for automatic exudates detection. *Biomedical Signal Processing and Control*, 2019, vol. 49, pp. 240–249. https://doi.org/10.1016/j.bspc.2018.12.004
12. Kouassi Nzoughet J., Guehlouz K., Leruez S., Gohier P., Bocca C., Muller J., Blanchet O., Bonneau D., Simard G., Milea D., Procaccio V., Lenaers G., de la Barca J.M.C., Reynier P. A data mining metabolomics exploration of glaucoma. *Metabolites*, 2020, vol. 10, no. 2, pp. 49. https://doi.org/10.3390/metabo10020049
13. Pang R., Labisi S.A., Wang N. Pigment dispersion syndrome and pigmentary glaucoma: overview and racial disparities. *Graefe's Archive for Clinical and Experimental Ophthalmology*, 2023, vol. 261, no. 3, pp. 601–614. https://doi.org/10.1007/s00417-022-05817-0
14. Wang X., Zhao Y., Pourpanah F. Recent advances in deep learning. *International Journal of Machine Learning and Cybernetics*, 2020, vol. 11, no. 4, pp. 747–750. https://doi.org/10.1007/s13042-020-01096-5
15. Domingues I., Pereira G., Martins P., Duarte H., Santos J., Abreu P.H. Using deep learning techniques in medical imaging: a systematic

Литература

1. Stitt A.W., Curtis T.M., Chen M., Medina R.J., McKay G.J., Jenkins A., Gardiner T.A., Lyons T.J., Hammes H.-P., Simó R., Lois N. The progress in understanding and treatment of diabetic retinopathy // Progress in Retinal and Eye Research. 2016. V. 51. P. 156–186. https://doi.org/10.1016/j.preteyeres.2015.08.001
2. Mahmoud M.H., Alamery S., Fouad H., Altinawi A., Youssef A.E. An automatic detection system of diabetic retinopathy using a hybrid inductive machine learning algorithm // Personal and Ubiquitous Computing. 2021. P. 1–15. https://doi.org/10.1007/s00779-020-01519-8
3. Dai L., Wu L., Li H., Cai C., Wu Q., Kong H., Liu R., Wang X., Hou X., Liu Y., Long X., Wen Y., Lu L., Shen Y., Chen Y., Shen D., Yang X., Zou H., Sheng B., Jia W. A deep learning system for detecting diabetic retinopathy across the disease spectrum // Nature Communications. 2021. V. 12. N 1. P. 3242. https://doi.org/10.1038/s41467-021-23458-5
4. Leung D.Y.L., Tham C.C. Normal-tension glaucoma: Current concepts and approaches — A review // Clinical & Experimental Ophthalmology. 2022. V. 50. N 2. P. 247–259. https://doi.org/10.1111/ceo.14043
5. French J.A., Lawson J.A., Yapici Z., Ikeda H., Polster T., Nabbout R., Curatolo P., de Vries P.J., Dlugos D.J., Berkowitz N., Voi M., Peyrard S., Pelov D., Franz D.N. Adjunctive everolimus therapy for treatment-resistant focal-onset seizures associated with tuberous sclerosis (EXIST-3): a phase 3, randomised, double-blind, placebo-controlled study // The Lancet. 2016. V. 388. N 10056. P. 2153–2163. https://doi.org/10.1016/s0140-6736(16)31419-2
6. Nazir T., Nawaz M., Rashid J., Mahum R., Masood M., Mehmood A., Ali F., Kim J., Kwon H.-Y., Hussain A. Detection of diabetic eye disease from retinal images using a deep learning based CenterNet model // Sensors. 2021. V. 21. N 16. P. 5283. https://doi.org/10.3390/s21165283
7. Barros D., Moura J.C., Freire C.R., Taleb A.C., Valentim R.A., Morais P.S. Machine learning applied to retinal image processing for glaucoma detection: review and perspective // BioMedical Engineering OnLine. 2020. V. 19. N 1. P. 20. https://doi.org/10.1186/s12938-020-00767-2
8. Ray J.S.R., Babu S.A., James J.W., Vedaiyan R. ARIMA based Time Series Analysis: Forecast COVID-19 Most Vaccinated Process and Active Cases classify using Probability Distribution Curve Rates (ARIMAPDC) // Proc. of the 2nd International Conference on Smart Electronics and Communication (ICOSEC). 2021. P. 546–551. https://doi.org/10.1109/ICOSEC51865.2021.9591774
9. Raj R.J.S., Babu Anantha S., Jegatheesan A., Arul Xavier V.M. A GAN-based triplet FaceNet detection algorithm using deep face recognition for autism child // Lecture Notes in Electrical Engineering. 2022. V. 905. P. 177–187. https://doi.org/10.1007/978-981-19-2177-3_18
10. Babu S.A., Joshua Samuel Raj R., Varalatchoumy M., Gopila M., Febiyola Justin B.V. Novel approach for predicting COVID-19 symptoms using ARM based APRIORI algorithm // Proc. of the 6th International Conference on Computing Methodologies and Communication (ICCMC). 2022. P. 1577–1580. https://doi.org/10.1109/ICCMC53470.2022.9753987
11. Khojasteh P., Aliahmad B., Kumar D.K. A novel color space of fundus images for automatic exudates detection // Biomedical Signal Processing and Control. 2019. V. 49. P. 240–249. https://doi.org/10.1016/j.bspc.2018.12.004
12. Kouassi Nzoughet J., Guehlouz K., Leruez S., Gohier P., Bocca C., Muller J., Blanchet O., Bonneau D., Simard G., Milea D., Procaccio V., Lenaers G., de la Barca J.M.C., Reynier P. A data mining metabolomics exploration of glaucoma // Metabolites. 2020. V. 10. N 2. P. 49. https://doi.org/10.3390/metabo10020049
13. Pang R., Labisi S.A., Wang N. Pigment dispersion syndrome and pigmentary glaucoma: overview and racial disparities // Graefe's Archive for Clinical and Experimental Ophthalmology. 2023. V. 261. N 3. P. 601–614. https://doi.org/10.1007/s00417-022-05817-0
14. Wang X., Zhao Y., Pourpanah F. Recent advances in deep learning // International Journal of Machine Learning and Cybernetics. 2020. V. 11. N 4. P. 747–750. https://doi.org/10.1007/s13042-020-01096-5
15. Domingues I., Pereira G., Martins P., Duarte H., Santos J., Abreu P.H. Using deep learning techniques in medical imaging: a systematic review of applications on CT and PET // Artificial Intelligence

review of applications on CT and PET. *Artificial Intelligence Review*, 2020, vol. 53, no. 6, pp. 4093–4160. https://doi.org/10.1007/s10462-019-09788-3
16. Aloysius N., Geetha M. A review on deep convolutional neural networks. *Proc. of the 2017 International Conference on Communication and Signal Processing (ICCSP)*, 2017, pp. 0588–0592. https://doi.org/10.1109/iccsp.2017.8286426
17. Yu Z., Jiang X., Zhou F., Qin J., Ni D., Chen S., Wang T. Melanoma recognition in dermoscopy images via aggregated deep convolutional features. *IEEE Transactions on Biomedical Engineering*, 2019, vol. 66, no. 4, pp. 1006–1016. https://doi.org/10.1109/tbme.2018.2866166
18. Ooi A.Z.H., Embong Z., Abd Hamid A.I., Zainon R., Wang S.L., Ng T.F., Hamzah R.A., Teoh S.S., Ibrahim H. Interactive blood vessel segmentation from retinal fundus image based on canny edge detector. *Sensors*, 2021, vol. 21, no. 19, pp. 6380. https://doi.org/10.3390/s21196380
19. Abdulsahib A.A., Mahmoud M.A., Mohammed M.A., Rasheed H.H., Mostafa S.A., Maashi M.S. Comprehensive review of retinal blood vessel segmentation and classification techniques: intelligent solutions for green computing in medical images, current challenges, open issues, and knowledge gaps in fundus medical images. *Network Modeling Analysis in Health Informatics and Bioinformatics*, 2021, vol. 10, no. 1, pp. 20. https://doi.org/10.1007/s13721-021-00294-7
20. Artaechevarria X., Munoz-Barrutia A., Ortiz-de-Solorzano C. Combination strategies in multi-atlas image segmentation: application to brain MR data. *IEEE Transactions on Medical Imaging*, 2009, vol. 28, no. 8, pp. 1266–1277. https://doi.org/10.1109/tmi.2009.2014372
21. Jia S., Jiang S., Lin Z., Li N., Xu M., Yu S. A survey: Deep learning for hyperspectral image classification with few labeled samples. *Neurocomputing*, 2021, vol. 448, pp. 179–204. https://doi.org/10.1016/j.neucom.2021.03.035
22. Sazak Ç., Nelson C.J., Obara B. The multiscale bowler-hat transform for blood vessel enhancement in retinal images. *Pattern Recognition*, 2019, vol. 88, pp. 739–750. https://doi.org/10.1016/j.patcog.2018.10.011
23. Alshaikhli T., Liu W., Maruyama Y. Automated method of road extraction from aerial images using a deep convolutional neural network. *Applied Sciences*, 2019, vol. 9, no. 22, pp. 4825. https://doi.org/10.3390/app9224825

Review. 2020. V. 53. N 6. P. 4093–4160. https://doi.org/10.1007/s10462-019-09788-3
16. Aloysius N., Geetha M. A review on deep convolutional neural networks // Proc. of the 2017 International Conference on Communication and Signal Processing (ICCSP). 2017. P. 0588–0592. https://doi.org/10.1109/iccsp.2017.8286426
17. Yu Z., Jiang X., Zhou F., Qin J., Ni D., Chen S., Wang T. Melanoma recognition in dermoscopy images via aggregated deep convolutional features // IEEE Transactions on Biomedical Engineering. 2019. V. 66. N 4. P. 1006–1016. https://doi.org/10.1109/tbme.2018.2866166
18. Ooi A.Z.H., Embong Z., Abd Hamid A.I., Zainon R., Wang S.L., Ng T.F., Hamzah R.A., Teoh S.S., Ibrahim H. Interactive blood vessel segmentation from retinal fundus image based on canny edge detector // Sensors. 2021. V. 21. N 19. P. 6380. https://doi.org/10.3390/s21196380
19. Abdulsahib A.A., Mahmoud M.A., Mohammed M.A., Rasheed H.H., Mostafa S.A., Maashi M.S. Comprehensive review of retinal blood vessel segmentation and classification techniques: intelligent solutions for green computing in medical images, current challenges, open issues, and knowledge gaps in fundus medical images // Network Modeling Analysis in Health Informatics and Bioinformatics. 2021. V. 10. N 1. P. 1–32. https://doi.org/10.1007/s13721-021-00294-7
20. Artaechevarria X., Munoz-Barrutia A., Ortiz-de-Solorzano C. Combination strategies in multi-atlas image segmentation: application to brain MR data // IEEE Transactions on Medical Imaging. 2009. V. 28. N 8. P. 1266–1277. https://doi.org/10.1109/tmi.2009.2014372
21. Jia S., Jiang S., Lin Z., Li N., Xu M., Yu S. A survey: Deep learning for hyperspectral image classification with few labeled samples // Neurocomputing. 2021. V. 448. P. 179–204. https://doi.org/10.1016/j.neucom.2021.03.035
22. Sazak Ç., Nelson C.J., Obara B. The multiscale bowler-hat transform for blood vessel enhancement in retinal images // Pattern Recognition. 2019. V. 88. P. 739–750. https://doi.org/10.1016/j.patcog.2018.10.011
23. Alshaikhli T., Liu W., Maruyama Y. Automated method of road extraction from aerial images using a deep convolutional neural network // Applied Sciences. 2019. V. 9. N 22. P. 4825. https://doi.org/10.3390/app9224825

Authors

Shanmugavel Anantha Babu — PhD, Associate Professor, Koneru Lakshmaiah Education Foundation, Hyderabad, 500075, Telangana, India, sc 57198087959, https://orcid.org/0000-0002-7446-0283, ananthmtech@gmail.com
Subramanian Murali — PhD, Associate Professor, Vellore Institute of Technology, Vellore, 632014, India, sc 55752705600, https://orcid.org/0000-0002-1631-8078, murali.s@vit.ac.in
Ellappan Vijayan — PhD, Associate Professor, Vellore Institute of Technology, Vellore, 632014, India, sc 57216300541, https://orcid.org/0000-0002-0207-0411, evijayan@vit.ac.in
Mahendran Anand — PhD, Associate Professor, Vellore Institute of Technology, Vellore, 632014, India, sc 56318694500, https://orcid.org/0000-0002-7629-9606, manand@vit.ac.in
Lakshmanan Ramanathan — PhD, Associate Professor, Vellore Institute of Technology, Vellore, 632014, India, sc 55808530000, https://orcid.org/0000-0002-1532-5495, lramanathan@vit.ac.in

Авторы

Ананта Бабу Шанмугавел — PhD, доцент, Университет Конеру Лакшмайан (KL), Хайдарабад, 500075, шт. Телангана, Индия, sc 57198087959, https://orcid.org/0000-0002-7446-0283, ananthmtech@gmail.com
Мурали Субраманиан — PhD, доцент, Технологический институт Веллуру, Веллуру, 632014, Индия, sc 55752705600, https://orcid.org/0000-0002-1631-8078, murali.s@vit.ac.in
Виджаян Эллаппан — PhD, доцент, Технологический институт Веллуру, Веллуру, 632014, Индия, sc 57216300541, https://orcid.org/0000-0002-0207-0411, evijayan@vit.ac.in
Ананд Махендран — PhD, доцент, Технологический институт Веллуру, Веллуру, 632014, Индия, sc 56318694500, https://orcid.org/0000-0002-7629-9606, manand@vit.ac.in
Раманатан Лакшманан — PhD, доцент, Технологический институт Веллуру, Веллуру, 632014, Индия, sc 55808530000, https://orcid.org/0000-0002-1532-5495, lramanathan@vit.ac.in

Received 23.11.2022
Approved after reviewing 26.04.2023
Accepted 27.05.2023

Статья поступила в редакцию 23.11.2022
Одобрена после рецензирования 26.04.2023
Принята к печати 27.05.2023